

# **X-Ray Absorption Spectroscopy Proves the Trigonal Planar Sulfur-Only Coordination of Cu(I) with High Affinity Tripodal Pseudopeptides.**

## **SUPPORTING INFORMATION**

Anne-Solène Jullien,<sup>a</sup> Christelle Gateau,<sup>a</sup> Isabelle Kieffer,<sup>b,c</sup>  
Denis Testemale,<sup>b,d</sup> Pascale Delangle<sup>a\*</sup>

<sup>a</sup> INAC, Service de Chimie Inorganique et Biologique (UMR\_E 3 CEA UJF), Commissariat à l'Énergie Atomique et aux Énergies Alternatives, 17 rue des martyrs, 38054 Grenoble cedex 9, France

\*E-mail: [pascale.delangle@cea.fr](mailto:pascale.delangle@cea.fr)

<sup>b</sup> BM30B/FAME beamline, ESRF, F-38043 Grenoble cedex 9, France

<sup>c</sup> Observatoire des Sciences de l'Université de Grenoble, UMS 832 CNRS Université Joseph Fourier, F-38041 Grenoble cedex 9, France

<sup>d</sup> Institut Néel, CNRS et Université Joseph Fourier, BP 166, F-38042, Grenoble Cedex 9, France

## PART 1: ORGANIC SYNTHESSES

**General information** - Solvents and starting materials were purchased from Aldrich, Acros, Fluka, Alfa Aesar, Bachem and used without further purification. All water solutions were prepared from ultrapure laboratory grade water that has been filtered and purified by reverse osmosis using Millipore MilliQ reverse-osmosis cartridge system (resistivity 18 M $\Omega$ .cm). Thin layer chromatography (TLC) was performed on silica gel 60 F254 (Merck). Flash chromatography was performed on silica gel 60 (40-63  $\mu$ m, Merck). Analytical and preparative HPLC were performed with a VWR system fitted with a purosphere RP18 column (Lichro CART<sup>®</sup> purospher star RP18, L = 250 mm,  $\varnothing$  = 4.6 mm and p = 5  $\mu$ m for analytical column; Hibar<sup>®</sup> purospher star RP18, L = 125 mm,  $\varnothing$  = 25 mm and p = 5  $\mu$ m for preparative column). Flow rates of 1 mL/min and 15 mL/min were used for analytical and preparative column, respectively. <sup>1</sup>H NMR and <sup>13</sup>C NMR spectra were recorded on a Varian Mercury 400 spectrometer and on a Bruker Avance 500 spectrometer. Chemical shifts ( $\delta$ ) are reported in ppm with the solvent as the internal reference, except for <sup>13</sup>C NMR spectra in D<sub>2</sub>O which are referenced to external DSS. Mass spectra were acquired with a Finigan LXQ-linear ion trap (THERMO Scientific, San Jose, USA) equipped with an electrospray source.

### Abbreviations

DMF: dimethylformamide

EDC: N-(3-Dimethylaminopropyl)-N'-ethylcarbodiimide hydrochloride

HOBt: 1-Hydroxybenzotriazole

NTA: nitrilotriacetic acid

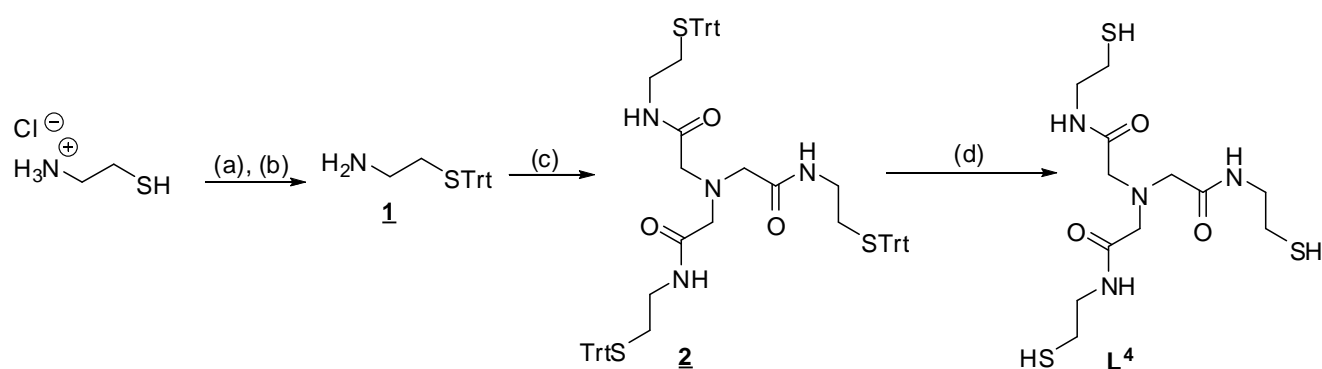
TFA: trifluoroacetic acid

TES: triethylsilane

*Note: Syntheses of L<sup>1</sup>, L<sup>2</sup> and L<sup>3</sup> were reported in reference [1].*

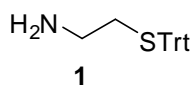
## Synthesis of NTA [Cysteamine]<sub>3</sub> [L<sup>4</sup>]

The tripodal architecture L<sup>4</sup> is built up starting from the commercially available cysteamine hydrochloride. The first step consists in a thiol protection with the trityl group followed by deprotonation of the hydrochloride using basic conditions. [2, 3] This reaction leads to **1** in 56 % yield. **1** is then involved in a coupling reaction with the NTA template to afford **2** in 90% yield. Eventually, a trityl deprotection is performed to afford L<sup>4</sup> in 66% yield. Thus, the synthesis of L<sup>4</sup> is achieved in four steps and 34% total yield.



**Scheme S1.** Synthesis of L<sup>4</sup> – reagents and conditions: a) (i) TrtCl, methylene chloride/ DMF, RT (ii) KOH, NaOH, Et<sub>2</sub>O, 56%; b) NTA, EDC, HOBt, RT, DMF, 90%; c) TFA/ TES, methylene chloride, RT, 66% (4 steps, 34% total yield).

**Compound 1** (adapted from the references [2] and [3])



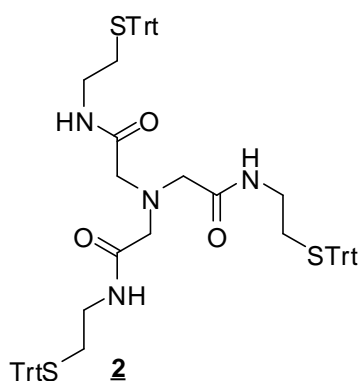
TrtCl (2.925 g, 10.5 mmol) was added to a solution of cysteamine hydrochloride (806 mg, 7.1 mmol) in a methylene chloride/ DMF mixture (5/5, v/v, 40 mL) at room temperature. After stirring for 2 hours at room temperature and concentration in vacuo, the resulting product was solubilized in a methylene chloride/water (5/5, v/v, 500 mL) mixture. The product was observed to form a white precipitate between the organic phase and the aqueous one, as a surfactant. The precipitate was isolated by filtration and dried in vacuo to provide the tritylcysteamine hydrochloride (1.579 g) as a white solid. This salt was solubilized in Et<sub>2</sub>O (270 mL) and aqueous KOH solution (17.5 mM, 100 mL). Then, aqueous NaOH solution (9.6 M) was added until no precipitate remains at the interface between the organic phase and the aqueous one. The same procedure was applied twice. Then, the organic layers were gathered,

dried over Na<sub>2</sub>SO<sub>4</sub>, filtrated and concentrated in vacuo. The resulting product **1** (1.258 g, 56% yield) was obtained as a white solid and used without purification.

<sup>1</sup>H NMR (CDCl<sub>3</sub>, 400 MHz, 298 K) δ 2.32 (t, *J* = 6.4 Hz, 2H, CH<sub>2</sub>S), 2.60 (t, *J* = 6.4 Hz, 2H, CH<sub>2</sub>N), 7.19-7.23 (m, 3H, 3H<sub>Ar</sub>), 7.26-7.30 (m, 6H, 6H<sub>Ar</sub>), 7.42-7.44 (m, 6H, 6H<sub>Ar</sub>)

ES-MS: *m/z*: 319.8 [M+H]<sup>+</sup>

## Compound **2**



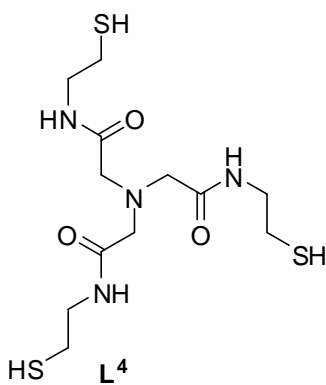
NTA (251 mg, 1.31 mmol) was added to a solution of **1** (1.258 g, 3.94 mmol) in DMF (37 mL) at room temperature. The resulting mixture was cooled at 0°C. Then EDC (790 mg, 4.12 mmol) and HOBT (555 mg, 4.10 mmol) were successively added. The resulting mixture was allowed to warm up at room temperature. After stirring for 6 hours at room temperature, the resulting mixture was evaporated in vacuo. The resulting crude product was diluted in water (500 mL) and extracted with ethyl acetate (4×500 mL). The combined organic layers were successively washed with saturated aqueous NaHCO<sub>3</sub> solution (250 mL) and brine (250 mL), then dried over Na<sub>2</sub>SO<sub>4</sub>, filtrated and concentrated in vacuo. The resulting product **2** (1.301 g, 90%) was obtained as a white solid and used without purification.

<sup>1</sup>H NMR (CDCl<sub>3</sub>, 400 MHz, 298 K) δ 2.33 (t, *J* = 6.4 Hz, 6H, 3×CH<sub>2</sub>S), 2.95 (td, *J* = 5.2 Hz, *J* = 6.4 Hz, 6H, 3×CH<sub>2</sub>N), 3.14 (s, 6H, 3×CH<sub>2</sub>CO), 6.79 (t, *J* = 5.2 Hz, 3H, 3×NH), 7.18-7.20 (m, 9H, 3 × 3H<sub>Ar</sub>), 7.23-7.29 (m, 18H, 3 × 6H<sub>Ar</sub>), 7.36-7-38 (m, 18H, 3 × 6H<sub>Ar</sub>)

<sup>13</sup>C NMR (CDCl<sub>3</sub>, 100 MHz, 298 K): δ 31.93 (3×CH<sub>2</sub>), 38.25 (3×CH<sub>2</sub>), 59.71 (3×CH<sub>2</sub>), 66.92 (3×C), 126.95 (9×CH-Ar), 128.12 (18×CH-Ar), 129.68 (18×CH-Ar), 144.75 (9×C), 170.06 (3×CO)

ES-MS: *m/z*: 1117.4 [M+Na]<sup>+</sup>

## Compound **L**<sup>4</sup>



TFA (0.75 mL, 9.8 mmol) and TES (0.3 mL, 1.88 mmol) were successively added to a solution of **2** (203 mg, 0.185 mmol) in methylene chloride (7 mL) at room temperature. After completion of the reaction (2 hours), the mixture was concentrated in vacuo. The resulting crude product was purified by preparative C18 reversed-phase HPLC (A: MeCN-water-TFA [90/10/0.1]; B: water-TFA [99.925/0.075]; A/B: 30/70 for 5 min, 30/70 to 100/0 for 7 min, 100/100 for 2 min,  $R_t = 6.4$  min) followed by lyophilisation to provide the compound **L**<sup>4</sup> (45 mg, 66%) as a white solid.

<sup>1</sup>H NMR (CD<sub>3</sub>CN, 400 MHz, 298 K)  $\delta$  1.71 (t,  $J = 8$  Hz, 3H, 3×SH), 2.62 (td,  $J = 6.4$  Hz,  $J = 8$  Hz, 6H, 3×CH<sub>2</sub>S), 3.28 (s, 6H, 3×CH<sub>2</sub>CO), 3.36 (q,  $J = 6.4$  Hz, 6H, 3×CH<sub>2</sub>N), 7.51 (s, broad, 3H, 3×NH)

<sup>13</sup>C NMR (CD<sub>3</sub>CN, 100 MHz, 298 K):  $\delta$  24.67 (3×CH<sub>2</sub>), 43.26 (3×CH<sub>2</sub>), 59.01 (3×CH<sub>2</sub>), 169.13 (3×CO)

ES-MS:  $m/z$ : 369.2 [M+H]<sup>+</sup>

*This compound is sensitive to air-oxidation. Therefore it was stored and manipulated in a glove box (Argon, O<sub>2</sub> < 1.2 ppm).*

## PART 2: XAS ANALYSES

EXAFS spectra were recorded on BM30B-FAME beamline at ESRF. [4, 5, 6]

### 2.1. Edge Analyses

The figure of edge analyses for  $L^1$  is presented in the core article (Figure 3). Here, the corresponding figure for  $L^2$  is depicted on Figure S1.

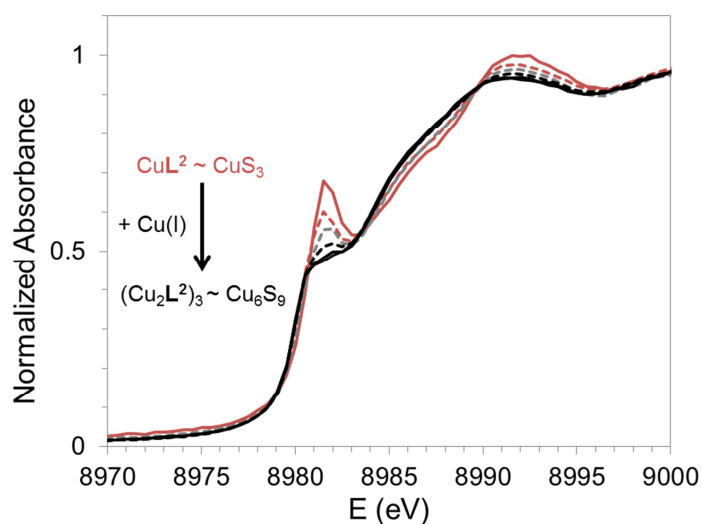


**Figure S1.** Normalized Cu edge spectra obtained for ligand  $L^2$  with increasing amounts of Cu(I). The peak intensity centered at 8982 eV decreases with the increase of Cu(I) concentration.

## 2.2. EXAFS Data Analyses

Data analysis was performed using the Horae package [7] including ATHENA for the data extraction and ARTEMIS for the shell fitting. Here, we aim at reporting the system of input coordinates [8] used in the Atoms module of Artemis, to calculate the Feff parameters, i.e. the effective scattering functions and mean free paths.

**Table S1.** Crystallographic data implemented in Atoms for Feff calculations (Space group  $P\bar{1}$ ,  $Z = 4$ ,  $V = 4616 \text{ \AA}^3$ ) [8]

### A. Lattice parameters

Lattice distances ( $\text{\AA}$ )	a =	12.1250	b =	17.1190	c =	24.2560
Lattice angles ( $^\circ$ )	$\alpha$ =	105.540	$\beta$ =	90.330	$\gamma$ =	107.480

### B. Atomic coordinates [8]

Atom	x	y	z
<b>Cu(1)</b>	0.3312	0.2038	0.1971
<b>Cu(2)</b>	0.3917	0.3393	0.1534
<b>Cu(3)</b>	0.1673	0.2675	0.1752
<b>Cu(4)</b>	0.2680	0.1893	0.0826
<b>S(1)</b>	0.5017	0.3119	0.2168
<b>S(2)</b>	0.1789	0.2144	0.2500
<b>S(3)</b>	0.3008	0.0874	0.1194
<b>S(4)</b>	0.2561	0.4076	0.1812
<b>S(5)</b>	0.3997	0.2933	0.0577
<b>S(6)</b>	0.0753	0.1871	0.0878

### **Fits based on shells described separately in a tetrahedral geometry**

The tetrahedral-based model consisted in using tetrahedral models as a basis for structural fitting in Artemis software (see core article). The  $k^3$ -weighted EXAFS spectra were Fourier transformed over the  $k$  range 2-13  $\text{\AA}^{-1}$  using a Hanning window. Fits were performed on the Fourier filtered spectra over the  $R$  range 1 -3  $\text{\AA}$ . For the mononuclear complexes, 3 sulfur atoms at a 2.25  $\text{\AA}$  sulfur-copper starting distance were defined within a tetrahedral geometry. For the clusters, 3 copper atoms were added at a 2.7  $\text{\AA}$  Cu-Cu starting distance, defining another shell in a tetrahedral geometry. The distances were fitted during the fit process. For both models, the amplitude factor  $So^2$  was set at 0.9 as for Cu(I) model compounds studied at BM30B FAME beamline [9] and the coordination numbers were set at 3 for both sulfur and copper shells. Other parameters were guess parameters accommodated during the fit process from the following initial values: the threshold energy shift  $\Delta E = 0$  eV; Debye-Waller factors  $\sigma^2 = 0.003 \text{\AA}^2$ ; distance variations or uncertainties  $\Delta r = 0 \text{\AA}$ .

As the coordinate-based model, the tetrahedral-based models match quite well the data for both the mononuclear species (Table S2) and the polynuclear ones (Table S3). Thus, the data confirm the formation of the  $\text{CuS}_3$  mononuclear species and the  $(\text{Cu}_2\text{L})_z$ -type clusters where the central copper is surrounded by three copper atoms in a distorted trigonal geometry and three copper atoms at an average distance of 2.7  $\text{\AA}$ .

The parameters reported in Tables S2-S3 are as follows: the reduced chi square  $\chi_n^2$  values (goodness of the fit), the deviation from the threshold energy  $E_0 = 8979$  eV reported as  $\Delta E$  (eV), the fitted distance Cu-S and Cu---Cu (Å), the Debye-Waller factors  $\sigma^2$  ( $10^3 \text{ \AA}^2$ ) and the R (%) factor related to the goodness of the fit.

**Table S2.** Tetrahedral-based model - EXAFS fitting results for the mononuclear complexes CuL ( $L^1, L^2$ ) (Table 1, samples 1A and 2A) ( $S_0^2 = 0.9$ )

CuL	$\chi_n^2$	$\Delta E$ (eV)	3S (Å)	$\sigma(S)^2$ ( $10^3 \text{ \AA}^2$ )	R (%)
$L^1$	15	4(2)	<b>2.23(1)</b>	5(1)	3.9
$L^2$	32	4(2)	<b>2.23(1)</b>	6(1)	7.0

**Table S3.** Tetrahedral-based model -EXAFS fitting results for the clusters  $[\text{Cu}_2\text{L}]_z$  ( $L^{1-4}$ ) (Table 1, samples 1F, 2H, 3A, 4A)

$(\text{Cu}_2\text{L})_x$	$\chi_n^2$	$\Delta E$ (eV)	$3 \times \text{Cu-S}$ (Å)	$\sigma_S^2$ ( $10^3 \text{ \AA}^2$ )	$3 \times \text{Cu-Cu}$ (Å)	$\sigma_{\text{Cu}}^2$ ( $10^3 \text{ \AA}^2$ )	R (%)
$L^1$	118	5(2)	<b>2.26(1)</b>	5(1)	<b>2.73(2)</b>	<b>15(3)</b>	7.0
$L^2$	51	4(2)	<b>2.26(1)</b>	5(1)	<b>2.74(2)</b>	<b>14(4)</b>	2.4
$L^3$	34	5(1)	<b>2.26(1)</b>	4(1)	<b>2.73(2)</b>	<b>10(1)</b>	2.5
$L^4$	16	5(1)	<b>2.26(1)</b>	4(1)	<b>2.73(2)</b>	<b>10(1)</b>	2.0

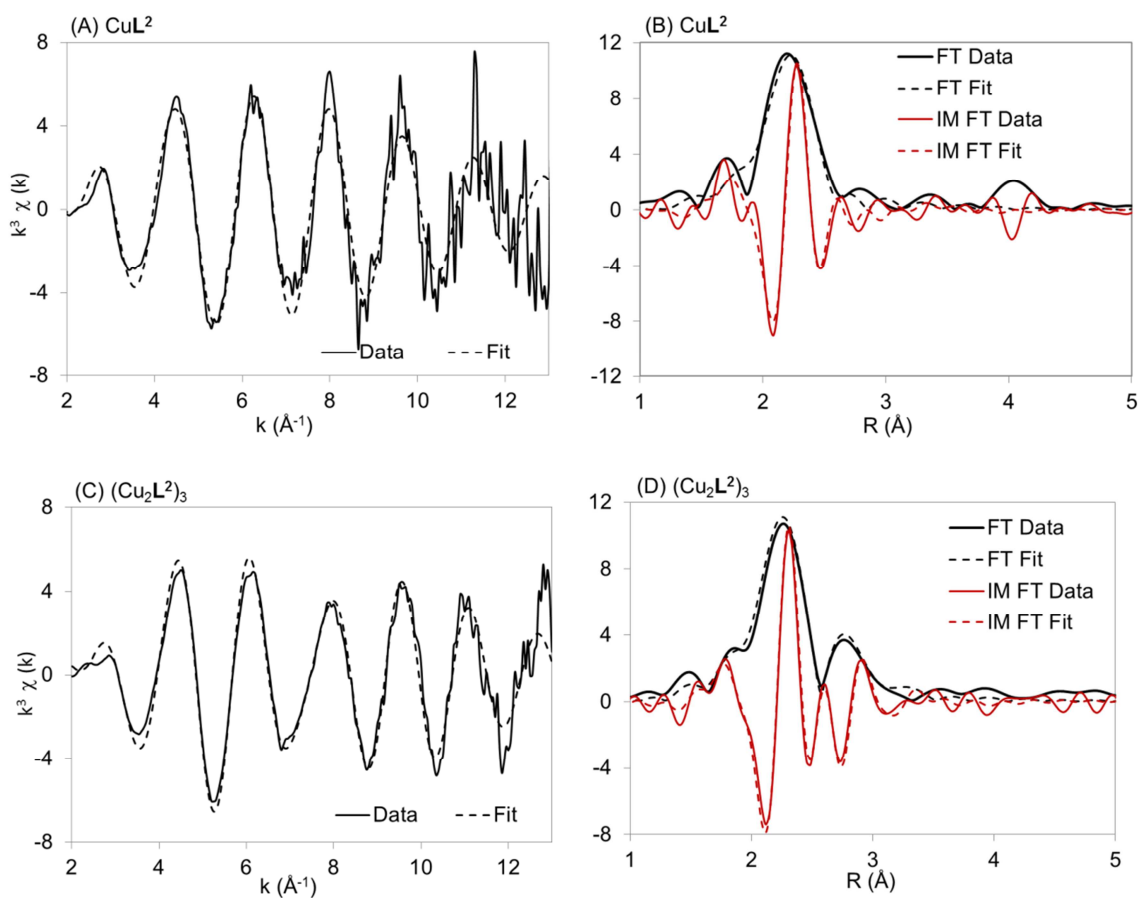


**Figure S2.** XAS data for CuL<sup>2</sup> (Sample 2A, Table 1) and (Cu<sub>2</sub>L<sup>2</sup>)<sub>3</sub> (Sample 2H, Table 1) and the corresponding fit (A), (C): Spectra of the  $k^3$ -weighted EXAFS experimental data and corresponding fit of CuL<sup>2</sup> (Sample 2A, Table 1) and the cluster (Cu<sub>2</sub>L<sup>2</sup>)<sub>3</sub> (Sample 2H, Table 1), respectively. (B), (D): Fourier transforms of the  $k^3$ -weighted EXAFS experimental data and corresponding fit of CuL<sup>2</sup> (Sample 2A, Table 1) and the cluster (Cu<sub>2</sub>L<sup>2</sup>)<sub>3</sub> (Sample 2H, Table 1), respectively.

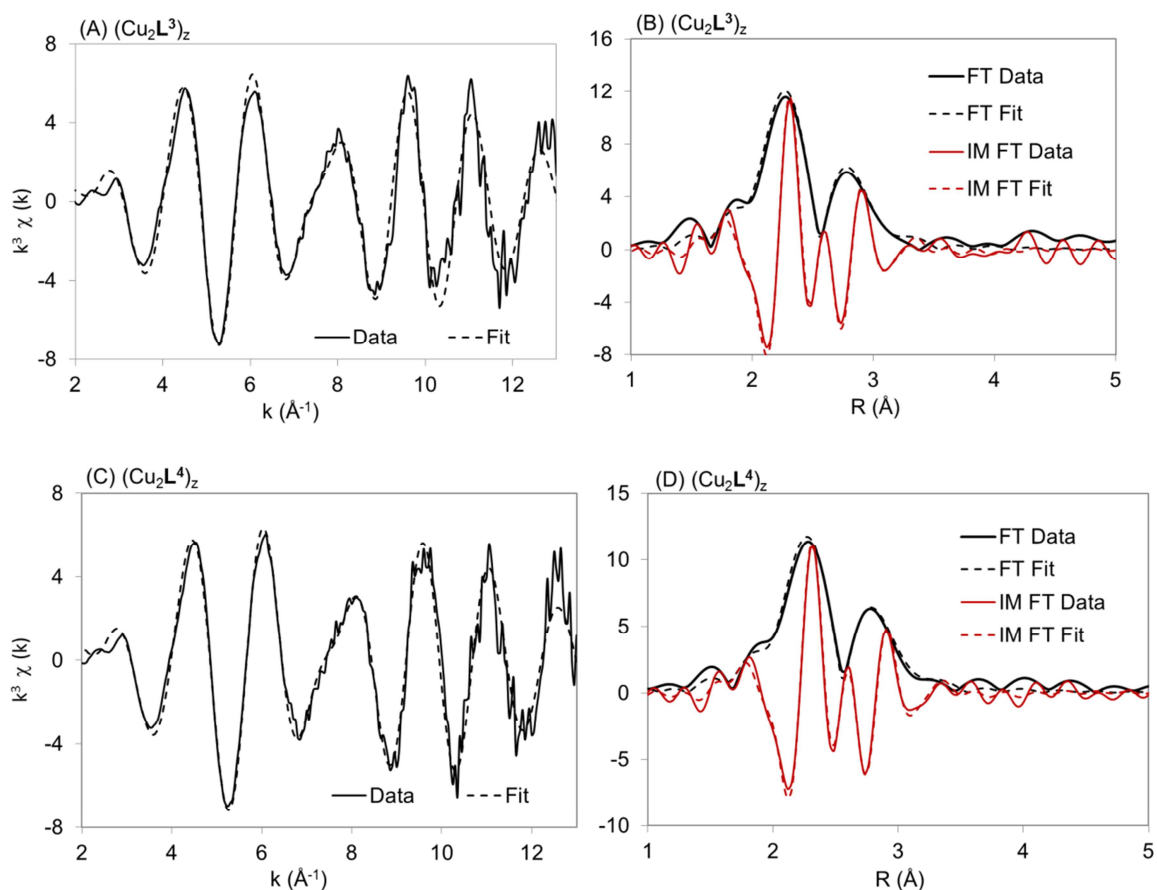


**Figure S3.** XAS data for clusters  $(\text{Cu}_2\text{L}^3)_z$  (Sample 3A, Table 1) and  $(\text{Cu}_2\text{L}^4)_z$  (Sample 4A, Table 1) and the corresponding fit (A), (C): Spectra of the  $k^3$ -weighted EXAFS experimental data and corresponding fit of  $(\text{Cu}_2\text{L}^3)_z$  (Sample 3A, Table 1) and  $(\text{Cu}_2\text{L}^4)_z$  (Sample 4A, Table 1) respectively. (B), (D): Fourier transforms of the  $k^3$ -weighted EXAFS experimental data and corresponding fit of  $(\text{Cu}_2\text{L}^3)_z$  (Sample 3A, Table 1) and  $(\text{Cu}_2\text{L}^4)_z$  (Sample 4A, Table 1) respectively.

### 2.3. Speciation of the Cu(I) species from XANES linear combination fits of the spectra for $L^1$ and $L^2$

**Table S4.** Percentage of mononuclear complex ( $x$ ) obtained by linear combinations (LC) of XANES spectra (LC tool available in Athena Software) for Cu(I) species with  $L^1$  (Table 1) and deduction of the equilibrium binding constant  $K_{63}$  using the affinity for the mononuclear complex  $\log\beta_{11}^{L^1} = 19.2$  reported in the literature [1] for the regular points of the curve (see Figure 7a).

Samples $L^1$	1A	1B	1C	1D	1E	1F
[Cu] <sub>0</sub>	0.0005	0.00125	0.002	0.0035	0.00425	0.00483
[L] <sub>0</sub>	0.00275	0.00268	0.00261	0.00246	0.00239	0.00243
[Cu] <sub>0</sub> /[L] <sub>0</sub>	0.18	0.47	0.77	1.42	1.78	1.99
$x = \% \text{CuL}$	1	0.836	0.606	0.24	0.156	0
[CuL]	0.0005	0.00105	0.00121	0.00084	0.000663	0
[Cu <sub>6</sub> L <sub>3</sub> ]	0	3.4E-05	0.00013	0.000443	0.000598	0.000805
[L]	0.00225	0.00153	0.001	0.00029	-	1.5E-05
[Cu]	1.4E-20	4.3E-20	7.6E-20	1.83E-19	-	0
$K_{63}$	-	7.2E+20	5.5E+20	4.97E+20	-	-
$\log K_{63}$	-	<b>20.86</b>	<b>20.74</b>	<b>20.70</b>	-	-

*Note: the concentrations are reported in molL<sup>-1</sup>. [Cu]<sub>0</sub>, [L]<sub>0</sub> are the total concentrations of copper and ligands respectively; [Cu], [L] are the concentrations of free copper and free ligands respectively;  $x = \% \text{CuL}$  is the fraction of CuL species in the sample; thus (1-x) is the fraction of Cu<sub>6</sub>S<sub>9</sub> species.*

**Table S5.** Percentage of mononuclear complex (x) obtained by linear combinations (LC) of XANES spectra (LC tool available in Athena Software) for Cu(I) species with  $L^2$  (Table 1) and deduction of the equilibrium binding constant  $K_{63}$  using the affinity for the mononuclear complex  $\log\beta_{11}^{L1} = 18.8$  reported in the literature [1] for the regular points of the curve (see Figure 7b). (List of parameters defined in Table S4)

Sample $L^2$	2A	2B	2C	2D	2E	2F	2G	2H
[Cu] <sub>0</sub>	0.0005	0.00074	0.00141	0.0015	0.0025	0.0035	0.0045	0.005
[L] <sub>0</sub>	0.00308	0.0029	0.00281	0.00297	0.00281	0.00275	0.00265	0.00247
[Cu] <sub>0</sub> /[L] <sub>0</sub>	0.16	0.26	0.50	0.51	0.89	1.27	1.70	2.02
x = % CuL	1	0.527	0.231	0.472	0.16	0.079	0	0
[CuL]	0.0005	0.00039	0.00033	0.00071	0.0004	0.000277	0	0
[Cu <sub>6</sub> L <sub>3</sub> ]	0	5.83E-05	0.00018	0.00013	0.00035	0.000537	0.00075	0.000833
[L]	0.00258	0.002335	0.00194	0.00187	0.00136	0.000862	0.0004	-
[Cu]	3.07E-20	2.65E-20	2.7E-20	6E-20	4.66E-20	5.09E-20	0	-
$K_{63}$	-	3.76E+21	6.5E+21	1.2E+21	3.78E+21	5.78E+21	-	-
$\log K_{63}$	-	<b>21.57</b>	<b>21.81</b>	<b>21.08</b>	<b>21.58</b>	<b>21.76</b>	-	-

## References

- [1] Pujol A.M., Gateau C., Lebrun C., Delangle P., *Chem. Eur. J.*, **2011**, *17*, 4418-4428.
- [2] Di Maro S., Pong R.C., Hsieh J.T., Anh J.M., *J. Med. Chem.*, **2008**, *51*, 6639-6641.
- [3] Van Der Vlies A.J., O'Neil C.P., Hasegawa U., Hammond N., Hubbell J.A., *Bioconj. Chem.*, **2010**, *21*, 653-662.
- [4] Proux O., Biquard X., Lahera E., Menthonnex J.J., Prat A., Ulrich O., Soldo Y., Trevisson P., Kapoudjyan G., Perroux G., Taunier P., Grand D., Jeantet P., Deleglise M., Roux J.P., Hazeman J.L., *Physica Scripta*, **2005**, *T115*, 970-973.
- [5] Hazeman J.L., Proux O., Nassif V., Palancher H., Lahera E., Da Silva C., Braillard A., Testemale D., Diot M.A., Alliot I., Del Net W., Manceau A., Gélébart F., Morand M., Permigny Q., Shukla A., *J. Synchrotron Rad.*, **2009**, *16*, 283-292.
- [6] Proux O., Nassif V., Prat A., Ulrich O., Lahera E., Biquard X., Menthonnex J., Hazemann J.L., *J. Synchrotron Rad.*, **2006**, *13*, 59-68.
- [7] Ravel B., Newville M., *J. Synchrotron Rad.*, **2005**, *12*, 537-541.
- [8] Baumgartner M., Schmalte H., Baerlocher C., *J. Solid State Chem.*, **1993**, *107*, 63-75.
- [9] Poger, D.; Fillaux, C.; Miras, R.; Crouzy, S.; Delangle, P.; Mintz, E.; Den Auwer, C.; Ferrand, M. *J. Biol. Inorg. Chem.* **2008**, *13*, 1239.